

Generating entanglement between quantum dots with different resonant frequencies based on Dipole Induced Transparency

Deepak Sridharan and Edo Waks

*Department of Electrical and Computer Engineering,
IREAP and JQI, University of Maryland,
College Park, Maryland 20742, USA*

Abstract

We describe a method for generating entanglement between two spatially separated dipoles coupled to optical micro-cavities. The protocol works even when the dipoles have different resonant frequencies and radiative lifetimes. This method is particularly important for solid-state emitters, such as quantum dots, which suffer from large inhomogeneous broadening. We show that high fidelities can be obtained over a large dipole detuning range without significant loss of efficiency. We analyze the impact of higher order photon number states and cavity resonance mismatch on the performance of the protocol.

PACS numbers:

I. 1. INTRODUCTION

Generation of entanglement between qubits is an important operation for a large variety of applications in quantum information processing. Such states can be used to realize schemes such as transmission of secret messages via quantum key distribution[1, 2] and teleportation of quantum information[3, 4, 5, 6]. The exchange of entanglement between two distant parties is also required for implementation of quantum repeaters [7] which use a combination of entanglement swapping and entanglement purification[8] to achieve unconditional secure communication over arbitrarily long distances.

To date, a variety of methods have been proposed for creating entanglement between spatially separated nodes. One of the most common methods is to transmit entangled photons generated by parametric down-conversion[9]. Entanglement protocols for atomic systems have also been proposed[10, 11, 12, 13, 14]. Atom entanglement has the advantages that quantum information can be stored for long time periods, which is important for long distance quantum networking.

Semiconductor based approaches to quantum information processing are currently an area of great interest because they offer the potential for a compact and scalable quantum information architecture. Furthermore, solid-state emitters such as semiconductor quantum dots (QDs), can be coupled to ultra-compact cavity waveguide systems to form highly integrated quantum systems [15, 16]. A major challenge in using solid-state emitters is that they suffer from enormous inhomogeneous broadening, typically caused by emitter size variation and strain fields in the host material. The inhomogeneous broadening makes it difficult to find two emitters with identical emission wavelengths. Protocols to date for generating atom entanglement require the dipoles to emit indistinguishable photons, and are thus difficult to implement in semiconductor systems. In order to implement quantum networking in semiconductors, we need a protocol that works even when the dipoles emit photons that are distinguishable.

In this paper, we describe a protocol for creating entanglement between two dipoles with different radiative properties, such as different emission wavelengths or radiative lifetimes. The proposed protocol uses Dipole Induced Transparency (DIT) to achieve the desired entanglement which occurs when a dipole is coupled to an optical cavity[17]. When the coupling is sufficiently strong, the dipole can switch a cavity from being highly transmitting to highly

reflecting. The switching contrast is determined by the atomic cooperativity, which is the ratio of the lifetime of the uncoupled emitter to the modified lifetime of the cavity-coupled emitter. Enhancement of spontaneous emission has been observed in semiconductor emitters coupled to a variety of different micro-cavity architectures[16, 18, 19, 20, 21, 22]. Modification of cavity reflectivity by coupling a quantum dot to a photonic crystal nanocavity has been recently observed[23, 24].

In section 2, we describe the basic protocol under idealized assumptions that all fields can be expanded to first order in photon number and that the two cavities have the same resonant frequencies. Section 3 then considers the effect of higher order photon number states on the efficiency and fidelity of entanglement. The impact of non-linear behavior away from the weak excitation limit is also discussed. In section 4 we investigate the effect of cavity frequency mismatch on the entanglement. Finally, in section 5 we perform a precise numerical simulation of the entanglement generation protocol for one specific implementation using the exciton bi-exciton cascade of a single Indium Arsenide(InAs) quantum dot. Numerical results from recent experimental work is used to show that this may be a promising method for achieving entanglement between two QDs for the first time.

II. 2. PROTOCOL FOR ENTANGLEMENT GENERATION

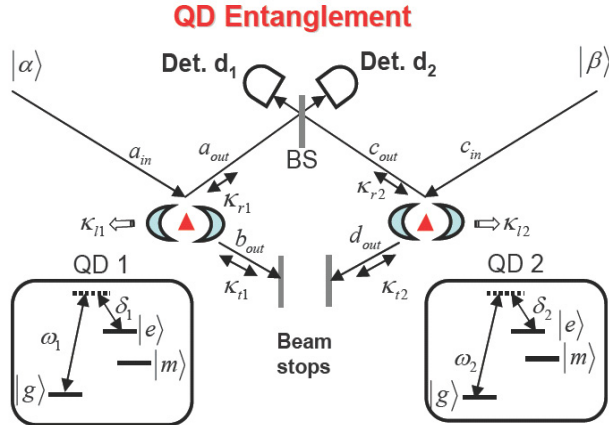


FIG. 1: Schematic of cavity waveguide system for generating entanglement between two spatially separated dipoles using DIT

The schematic for generating entanglement between two spatially separated dipoles that

emit distinguishable photons is shown in Fig 1. Each qubit consists of a dipole coupled to a double sided cavity. Each dipole is assumed to have three states: a ground state, a long lived metastable state and an excited state, which we refer to as $|g\rangle$, $|m\rangle$ and $|e\rangle$ respectively. The states $|g\rangle$ and $|m\rangle$ represent the two qubit states of the dipole. The transition from the ground state to the excited state for dipole 1, may be detuned by δ_1 from the resonant frequency ω_1 of cavity 1. Similarly, the transition from the ground state to the excited state for dipole 2 may be detuned by δ_2 from the resonant frequency ω_2 of cavity 2. We assume that when the dipole is in state $|g\rangle$ it couples to the cavity mode via an optical transition to state $|e\rangle$, while when it is in state $|m\rangle$ it does not optically couple to the cavity mode. State $|m\rangle$ may be decoupled from the cavity due to either spectral detuning or selection rules. Although state $|m\rangle$ is illustrated in the diagram as having an energy level that is in between states $|g\rangle$ and $|e\rangle$, this is not required. The only requirement is that when the dipole is in state $|m\rangle$ it is decoupled from the cavity. This point will be analyzed in more detail when we consider using the exciton-biexciton transitions of an InAs QD to achieve entanglement. The desired level structure described above can be realized in a variety of solid-state material systems. In semiconductor quantum dots one can use the exciton and biexciton transitions[25], as well as the spin-based bright and dark exciton states[26]. In addition, three level structures can also be achieved using quantum-dot molecules[27], charged quantum dots[28] and impurity bound excitons[29]. Similar qubits states could also be realized in other materials such as diamond using neutral and negatively charged nitrogen vacancy defects[30, 31].

The decay rates of the two dipoles is given by γ_1 and γ_2 respectively. To characterize the interaction between the dipoles and the cavity modes, we define the operators $\hat{\sigma_{1-}}$ and $\hat{\sigma_{2-}}$. They represent the dipole lowering operators for the dipoles in cavities 1 and 2 respectively. It should be noted that $\hat{\sigma_{1-}}$ and $\hat{\sigma_{2-}}$ represent the dipole lowering operators for the g-e transition. Although state $|m\rangle$ is decoupled from the cavity, we still define the dipole operators $\hat{\sigma_{m1-}}$ and $\hat{\sigma_{m2-}}$ for the dipole in state $|m\rangle$. These dipole are detuned by δ_{m1} and δ_{m2} from their respective cavities.

We define $\hat{\mathbf{a}}_{in}$ and $\hat{\mathbf{c}}_{in}$ as the two input modes, $\hat{\mathbf{a}}_{out}$ and $\hat{\mathbf{c}}_{out}$ as the reflected modes, and $\hat{\mathbf{b}}_{out}$ and $\hat{\mathbf{d}}_{out}$ as the transmitted modes to the two cavities, as illustrated in Fig. 1. The energy decay rate of cavity 1 into the reflected and transmitted modes is given by κ_{r1} and κ_{t1} respectively. Similarly, the energy decay rates of cavity 2 into the reflected and transmitted

modes is given by κ_{r2} and κ_{t2} respectively. There is also the decay rate κ_{l1} and κ_{l2} into the parasitic leaky modes that is due to losses such as material absorption and out of plane scattering. The field inside the cavities are represented by the cavity field operators $\hat{\mathbf{f}}_1$ and $\hat{\mathbf{f}}_2$.

The protocol works as follows. Both the dipoles are initialized to be in an equal superposition of qubit states $|g\rangle$ and $|m\rangle$. This can be achieved by first driving the dipoles into the lowest energy state by either waiting several radiative lifetimes or optical pumping. The qubit state can then be rotated by either a direct $\pi/2$ transition, or a raman transition[32]. The choice of method depends on the specifics of the dipole and material system. Once the initialization step is complete, the initialized state of the two dipole system is given by $1/2(|gg\rangle + |mm\rangle + |gm\rangle + |mg\rangle)$.

After the initialization of the dipoles, a weak coherent field $|\alpha\rangle$ with frequency ω is inserted at input $\hat{\mathbf{a}}_{in}$. Simultaneously, another weak coherent field $|\beta\rangle$ that is phase coherent with $|\alpha\rangle$ (i.e. originates from a common laser source) is injected at $\hat{\mathbf{c}}_{in}$. These input fields interact with the cavity-dipole system. The interaction between the input field $\hat{\mathbf{a}}_{in}$ and cavity-dipole system 1 can be characterized by the Heisenbergs equations of motion for the cavity field operator $\hat{\mathbf{f}}_1$ and the dipole lowering operator $\hat{\sigma}_{1-}$

$$\begin{aligned} \frac{d\hat{\mathbf{f}}_1}{dt} &= -(i\omega_0 + (\kappa_{r1} + \kappa_{t1} + \kappa_{l1})/2)\hat{\mathbf{f}}_1 - \sqrt{\kappa_{r1}}\hat{\mathbf{a}}_{in} - ig\hat{\sigma}_{1-} - ig\hat{\sigma}_{m1-} \\ \frac{d\hat{\sigma}_{1-}}{dt} &= (-i(\omega_0 + \delta_1) + \gamma_1)\hat{\sigma}_{1-} + ig\hat{\sigma}_{z1}\hat{\mathbf{f}}_1 \\ \frac{d\hat{\sigma}_{m1-}}{dt} &= (-i(\omega_0 + \delta_{m1}) + \gamma_1)\hat{\sigma}_{m1-} + ig\hat{\sigma}_{zm1}\hat{\mathbf{f}}_1 \end{aligned} \quad (1)$$

Similar equations can also be written for the interaction of the input field $\hat{\mathbf{c}}_{in}$ with cavity-dipole system 2.

The interaction between the input fields and the cavity-dipole systems results in part of the field being transmitted into the modes $\hat{\mathbf{b}}_{out}^\dagger$ and $\hat{\mathbf{d}}_{out}^\dagger$, while the remainder is reflected into the modes $\hat{\mathbf{a}}_{out}^\dagger$ and $\hat{\mathbf{c}}_{out}^\dagger$, or absorbed by the QD. The amount of light reflected and transmitted is given by the cavity reflection and transmission coefficients. Our analysis works in the weak excitation limit, where predominantly the quantum dots are populated in the ground state. In this limit, $\langle\hat{\sigma}_{z1}(t)\rangle \approx -1$. This also implies that the population inversion for the dipole in state $|m\rangle$ is close to 0 i.e. $\langle\hat{\sigma}_{zm1}(t)\rangle \approx 0$ Using this limit in Eq. 1, we can derive the reflection and transmission coefficients to be[33]

$$\begin{aligned}
r_1(\omega) &= \frac{(-i\Delta\omega_1 + \frac{g^2}{-i(\Delta\omega_1 - \delta_1) + \gamma_1}) + (\kappa_{r1} - \kappa_{t1} - \kappa_{l1})/2}{(-i\Delta\omega_1 + (\kappa_{r1} + \kappa_{t1} + \kappa_{l1})/2 + \frac{g^2}{-i(\Delta\omega_1 - \delta_{1,2}) + \gamma_1})} \\
t_1(\omega) &= \frac{\sqrt{\kappa_{r1}\kappa_{t1}}}{(-i\Delta\omega_1 + (\kappa_{r1} + \kappa_{t1} + \kappa_{l1})/2 + \frac{g^2}{-i(\Delta\omega_1 - \delta_1) + \gamma_1})}
\end{aligned} \tag{2}$$

where $\Delta\omega_1 = \omega - \omega_1$. These equations are obtained for cavity-dipole system 1. The reflection and transmission coefficients for dipole 2 are identical to dipole 1 in form, and are obtained by substituting the dipole 2 parameters into Eq. 2.

To get a better feel for Eq. 2, it is helpful to first consider the simplified case where $\Delta\omega_1 = 0$. Assume first that the dipole is in state $|g\rangle$ and that the g-e transition is resonant with the cavity such that $\delta_1 = 0$. We see that maximum reflection and minimum transmission occurs for the case when $\kappa_{r1} = \kappa_{t1} + \kappa_{l1}$, called the critical coupling condition. This condition ensures that no light is reflected from the cavity when the incident field is directly on cavity resonance. We represent the decay rate κ_{r1} at critical coupling as κ_1 . Hence, the transmission and reflection coefficients simplify to $t = 1/(1+C)$ and $r = C/(1+C)$, where $C = g^2/\gamma_1\kappa_1$ is called the atomic cooperativity. If $C \gg 1$, which is the desired operation regime, then $r=1$ and all of the light is reflected. Now suppose the dipole is instead in state $|m\rangle$ which is detuned from the cavity by δ_m . We then have $t = 1/(1+CL)$ and $r = CL/(1+CL)$, where $L = \gamma_1/(\gamma_1 + i\delta_m)$ is a Lorentzian function. If we assume that either state $|m\rangle$ is highly detuned from the resonance of the g-e transition ($\delta_m \gg g^2/\kappa_1$) or the transition is very weak due to selection rules ($C \approx 0$), then $t=1$ and now the light is completely transmitted. Thus, by changing the state of the dipole from $|g\rangle$ to $|m\rangle$ we can completely change the reflectivity of the cavity.

In a realistic system we cannot assume that the two dipoles are resonant with their respective cavities, since in general they will have different resonant frequencies. Nor can we assume the reflection and transmission coefficients will reach their ideal limits because δ_m is not infinitely large and we usually don't have perfect selection rules to cancel out the m-e transition. In this case we define for dipole 1, t_1^g and r_1^g as the transmission and reflection coefficients when the dipole is in state $|g\rangle$, and t_1^m and r_1^m when the dipole is in state $|m\rangle$. We define r_2^g, t_2^g, r_2^m , and t_2^m analogously for dipole 2. These coefficients can be calculated by plugging in the appropriate values corresponding to the different transitions of the dipoles. It is important to emphasize that we do not assume that the δ , g , γ , and κ are the same for

both dipoles. The protocol we describe works even if all of these parameters are different, which is why it is so useful in semiconductors.

Before continuing, it is worth noting that in much of the literature the atomic cooperativity C is often interchanged with the Purcell factor, defined as the ratio of the lifetime of the dipole inside the cavity to that of a dipole in bulk or free space, which we denote γ_{bulk} . Although the atomic cooperativity is the correct parameter to use in the strictest sense, it is a very difficult parameter to measure. The Purcell factor in contrast is easier to measure and almost always gives a lower bound on the parameter C in any realistic system. The reason for this is that γ_{bulk} is due both to radiative and non-radiative decay. In contrast the decay rate γ is the decay rate into non-cavity modes and is mainly due to non-radiative processes, as radiation into modes other than the cavity mode is highly suppressed. Thus, outside of some atypical cases where the cavity has two modes resonant with the QD, we expect that $\gamma_{bulk} > \gamma$. Therefore, in virtually all cases C can be replaced by the Purcell factor to get a lower bound on the performance of the system.

We first investigate the protocol under the assumptions that the resonant frequencies of both the cavities are the same($\omega_1 = \omega_2$), and the input fields $|\alpha\rangle$ and $|\beta\rangle$ are sufficiently weak that we may expand them to first order in photon number. The initial state of the system(dipoles and fields) is given by $|\Psi_i\rangle = 1/2(|gg\rangle + |mm\rangle + |gm\rangle + |mg\rangle)(\alpha\hat{\mathbf{a}}_{in}^\dagger + \beta\hat{\mathbf{c}}_{in}^\dagger)$. The fields, after interacting with the cavities, are transformed according to cavity reflection and transmission coefficients. That is, if dipole 1 is in state $|g\rangle$ then $\hat{\mathbf{a}}_{in} \rightarrow r_1^g\hat{\mathbf{a}}_{out} + t_1^g\hat{\mathbf{b}}_{out}$, and if it is in state $|m\rangle$ then $\hat{\mathbf{a}}_{in} \rightarrow r_1^m\hat{\mathbf{a}}_{out} + t_1^m\hat{\mathbf{b}}_{out}$. The transformation for photon in $\hat{\mathbf{c}}_{in}$ and dipole 2 is defined in a completely analogous way. The reflected fields from the two cavities are mixed on a 50/50 beamsplitter that applies the transformation: $\hat{\mathbf{a}}_{out}^\dagger \rightarrow (\hat{\mathbf{d}}_1 + \hat{\mathbf{d}}_2)/\sqrt{2}$, $\hat{\mathbf{c}}_{out}^\dagger \rightarrow (\hat{\mathbf{d}}_1 - \hat{\mathbf{d}}_2)/\sqrt{2}$. The final state of the QDs can be obtained by applying the cavity and beamsplitter transformations. If a detection event is observed in detector $\hat{\mathbf{d}}_2$, then the state of the two QDs collapses to

$$|\Psi_f\rangle = \frac{1}{N}[(\alpha r_1^g - \beta r_2^g)|gg\rangle + \alpha r_1^g|gm\rangle - \beta r_2^g|mg\rangle] \quad (3)$$

where $N^2 = |\alpha r_1^g - \beta r_2^g|^2 + |\alpha r_1^g|^2 + |\beta r_2^g|^2$.

In general, $r_1^g \neq r_2^g$ because the dipoles have different resonant frequencies. However, we can correct for this mismatch by properly adjusting the amplitudes of the fields. If the

amplitudes are selected such that

$$\alpha r_1^g = \beta r_2^g \quad (4)$$

the state of the qubits is projected onto $|\Psi_-\rangle = (|gm\rangle - |mg\rangle)/\sqrt{2}$ which is an ideal entangled state. Thus, by properly choosing the amplitude and phase of the input coherent fields $|\alpha\rangle$ and $|\beta\rangle$, we ensure that a detection at $\hat{\mathbf{d}}_2$ creates an entangled state of dipoles. Note that the entanglement generation is accomplished despite the fact that the two dipoles may have completely different resonant frequencies or decay rates.

III. 3. HIGHER ORDER PHOTON NUMBERS

The matching condition $\alpha r_1^g = \beta r_2^g$ as given in Eq 4 gives a relationship between α and β , but does not tell us how large to make α . In general, we want to make $|\alpha|^2$ as large as possible to improve the chances of a detection event at $\hat{\mathbf{d}}_2$. The probability of detecting a photon at detector $\hat{\mathbf{d}}_2$ is defined as the efficiency η of the protocol. When the fields $|\alpha\rangle$ and $|\beta\rangle$ are weak, efficiency of the protocol is proportional to the intensity of the field at $\hat{\mathbf{d}}_2$ and can be derived to be $|\alpha r_1^g|^2/4$. The factor 1/4 appears because 50% of the field is transmitted into the modes $\hat{\mathbf{b}}_{out}^\dagger$ and $\hat{\mathbf{d}}_{out}^\dagger$ and another 50% is lost when the beamsplitter splits the photons equally between $\hat{\mathbf{d}}_1$ and $\hat{\mathbf{d}}_2$. We see that we can achieve higher efficiencies by increasing input photon flux rate $|\alpha|^2$. However, if we make α too large we can no longer expand the fields to first order in photon number and higher order photon number contributions will become important.

Higher order photon number contributions are undesirable because they serve as a decoherence mechanism. In the ideal case where only one photon is injected into the system, a detection event at $\hat{\mathbf{d}}_2$ ensures that there are no other photons in the system which may carry "which path" information about the state of the dipole. Now suppose we consider the second order process of simultaneously injecting two photons into the input ports $|\alpha\rangle$ and $|\beta\rangle$. In the ideal case (both dipoles are on resonance with the cavities), if the state of the two dipoles is $|gm\rangle$, cavity 1 will reflect its incident photon while cavity 2 will transmit the second photon. The transmitted photon in cavity 2 will always keep track of the fact that dipole 2 was in state $|m\rangle$, and this information cannot be erased by the beamsplitter. Thus, we expect the state to be completely decohered when this happens.

We will now consider not only this specific case, but full expansion of the coherent fields

α and β to all photon numbers to see how the final state of the system is affected. The initial state of the system is given by $|\Psi_i\rangle = 1/2(|gg\rangle + |mm\rangle + |gm\rangle + |mg\rangle|\alpha\rangle|\beta\rangle)$. The coherent states $|\alpha\rangle$ and $|\beta\rangle$ can also be written as $|\alpha\rangle = D_1(\alpha)|0\rangle$ and $|\beta\rangle = D_2(\beta)|0\rangle$. D_1 and D_2 are the displacement operators and are given by

$$\begin{aligned} D_1(\alpha) &= e^{\alpha\hat{\mathbf{a}}_{in}^\dagger - \alpha^*\hat{\mathbf{a}}_{in}} \\ D_2(\beta) &= e^{\beta\hat{\mathbf{c}}_{in}^\dagger - \beta^*\hat{\mathbf{c}}_{in}} \end{aligned} \quad (5)$$

The displacement operator provides as convenient way of writing the coherent states and includes all the higher order photon numbers contributions.

The final state of system $|\Psi_f\rangle$ can be obtained by applying the cavity and beamsplitter transformations to the initial state $|\Psi_i\rangle$. After applying the transformations, the final state of the QDs is obtained by tracing out over the photon fields conditioned on a detection event at detector $\hat{\mathbf{d}}_2$. The state of the dipoles is therefore given by the reduced density matrix

$$\rho_{dipoles} = \frac{tr_{(fields)}\{\langle M|\Psi_f\rangle\langle\Psi_f|M\rangle\}}{tr_{(dipoles\&fields)}\{\langle M|\Psi_f\rangle\langle\Psi_f|M\rangle\}} \quad (6)$$

The matrix $M = \sum_{n=1}^{\infty} |n\rangle_{d_2}\langle n|$ is a positive projector that projects the state of the system onto a subspace containing at least one photon in $\hat{\mathbf{d}}_2$. This projection models the measurement performed by the photon counter, which registers a detection event as long as there is at least one photon in the detection mode.

Since the final state of QDs is mixed, we need a figure of merit to measure how well the QDs are entangled. In this paper we use the fidelity, which is defined as the overlap integral between the desired final state and the actual final state of the system. In our protocol, the desired final state is the maximally entangled Bell state $|\Psi_-\rangle$. Thus, the expression for fidelity is $\langle\Psi_-|\rho_{dipoles}|\Psi_-\rangle$. If the actual final state is same as the desired final state, we have a perfect entangled state and a fidelity of 1. A fidelity of 0.5 implies that the state of the QDs is a random mixture of $|gm\rangle$ and $|mg\rangle$ and completely decohered. An analytical expression for the fidelity can be calculated by evaluating $\rho_{dipoles}$ and averaging over the state $|\Psi_-\rangle$. We have carried out this calculation, but the expression for the fidelity is messy and the math is involved. The procedure for calculating the fidelity along with the final analytical expression are given in Appendix A. The expression in the appendix is used for subsequent calculations of fidelity.

We also define the efficiency η as the probability of getting a detection at detector $\hat{\mathbf{d}}_2$.

Mathematically this is given by the expression, $\eta = \text{tr}_{(\text{dipoles\&fields})}\{\langle M|\Psi_f\rangle\langle\Psi_f|M\rangle\}$. Using the matching condition $\alpha r_1^g = \beta r_2^g$, the expression can be simplified to $\eta = 0.5(1 - e^{|\alpha r_1^g|^2/2})$.

For the calculations in this paper, we use parameters that are appropriate for InAs quantum dots coupled to photonic crystal defect cavities. We represent the total decay rate out of each cavity $\kappa_{r1} + \kappa_{t1} + \kappa_{l1}$ and $\kappa_{r2} + \kappa_{t2} + \kappa_{l2}$ as κ and set it to be equal to 100 GHz. This corresponds to a cavity Q of 3300. We set $g = 20$ GHz for both the quantum dots. We estimate dipole decay rate γ within the cavity to be 0.125 GHz, using reported data that measured the lifetime of several quantum dots that were placed inside a photonic crystal cavity, but heavily detuned [34]. Using these values we calculate C to be 32 and the cavity-dipole systems to be 96.7% reflective on resonance. For the chosen values of g and κ , the cavity-dipole systems are in the weak coupling regime($g < \kappa/4$). However, the analysis in this paper is completely general and is equally valid also for the strong coupling regime. In Fig 2, we plot both fidelity and efficiency as a function of $|\alpha r_1^g|^2$. Fidelity is plotted for four values of δ_1/κ , ranging from 0 to 1, with δ_2 fixed at 0. Note that the efficiency is only a function of $|\alpha r_1^g|$, so the plot of efficiency is the same for all values of δ_1 . From Fig 2, we see that there is a tradeoff between fidelity and efficiency as we increase α . When $|\alpha r_1^g|^2 \ll 1$ the fidelity is close to 1, indicating an ideal entangled state, which is consistent with our predictions in the weak field limit. In the region $0.1 < |\alpha r_1^g|^2 < 1$, the fidelity quickly drops due to the presence of higher photon number contributions. In the limit $|\alpha r_1^g|^2 \gg 1$, the fidelity asymptotically approaches 0.5, indicating the higher photon number contributions have completely decohered the state.

When $|\alpha r_1^g|^2 \ll 1$, the fidelity curves for different values of δ_1 nearly overlap. Fidelity stays close to 1 in this region. However, in the region $0.1 < |\alpha r_1^g|^2 < 1$, the fidelity curves for different values of δ_1 separate out. There is a drop in fidelity with increase in dipole detuning from $\delta_1 = 0$ to $\delta_1 = \kappa$. Also, efficiency is a function of $|\alpha r_1^g|$ alone and does not change with δ_1 . This implies that fidelity decreases with increase in dipole detuning for a constant efficiency.

In Fig 2, we also plot a line of constant fidelity of 0.85. Note that for every value of δ_1 there is a unique point on the plot corresponding to a fidelity of 0.85. As δ_1 increases, this point shifts to lower values of $|\alpha r_1^g|^2$. Since, efficiency is a function of $|\alpha r_1^g|$, this in turn implies a decrease in efficiency. Thus, it is important to consider how the efficiency of the protocol changes for a fixed value of fidelity.

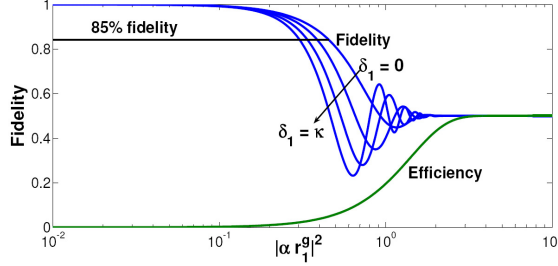


FIG. 2: Variation of fidelity and efficiency with $|\alpha r_1^g|^2$ for different values of δ_1 .

To investigate this, we plot efficiency as a function of δ_1/κ for several values of δ_2 for a constant fidelity of 0.85 in Fig 3. We see that even though there is a loss of efficiency, the change is gradual and there is only a 50% reduction over a cavity linewidth. Also, we would expect that if we added another detuning δ_2 , efficiency would decrease. However, this does not happen. From Fig 3 we see that the effect of δ_2 is to shift the efficiency curves by the detuning δ_2 without altering the shape. So, the protocol can be used to obtain high efficiencies over a wide range of dipole detunings.

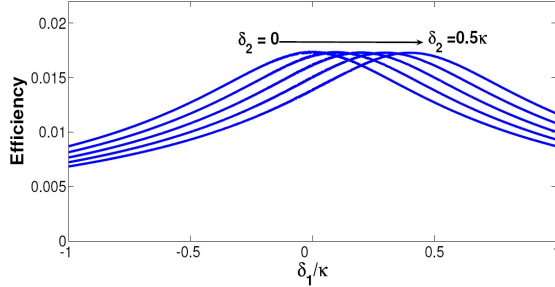


FIG. 3: Efficiency as a function of δ_1/κ for different δ_2 . Fidelity is fixed at 0.85

IV. 4. VALIDITY OF WEAK EXCITATION LIMIT

In the protocol we describe, dipole detuning is compensated by adjusting the amplitude and phase of the input coherent fields until the matching condition $\alpha r_1^g = \beta r_2^g$ is satisfied. The more detuning we have, the larger the amplitude required by the coherent field in order to achieve the desired efficiency. It is possible that at some point, the amplitudes required by the coherent fields will be so large that the g-e transition of the QDs will be saturated leading to an optical nonlinearity and linewidth broadening[35]. Because of this, the cavity

reflection and transmission equations will depend on the pump power and Eq 2 needs to be modified accordingly. However, our protocol is intended to work in the linear regime wherein the QDs are unsaturated. This is possible only if the amplitude of the input fields is within a certain limit called the weak excitation limit. The weak excitation limit is defined as $\langle \sigma_z(t) \rangle \approx -1$, which is equivalent to the statement $\langle \sigma_+ \sigma_- \rangle \ll 1$. and is necessary for Eq. 2 to be valid. This condition puts a constraint on the operation of the protocol.

In order to investigate the implication of the weak excitation constraint, we start with the Heisenbergs equation of motion for the cavity field operator \hat{f}_1 and the dipole lowering operator $\hat{\sigma}_-$ given in Eq 1. We will consider cavity-dipole system 1. Similar equations are also applicable for cavity-dipole system 2.

Eliminating \hat{b} from Eq 1, we have

$$[\frac{\kappa}{2}(i\delta_1 + \gamma) - g^2]\hat{\sigma}_- = -ig\sqrt{\kappa}\hat{a}_{in}^\dagger \quad (7)$$

Using the fact the cooperativity index C is $g^2/\gamma\kappa > 1$, the equation can be further simplified and multiplied with its conjugate to obtain

$$\langle \sigma_+ \sigma_- \rangle = \frac{g^2 \kappa}{(g^4 + \delta_1^2 \kappa^2/4)} \langle \hat{a}_{in}^\dagger \hat{a}_{in} \rangle \quad (8)$$

The parameter $\langle \sigma_+ \sigma_- \rangle$ represents the probability of the QD being in the excited state. In the weak excitation limit, $\langle \sigma_+ \sigma_- \rangle \ll 1$. We also identify $\langle \hat{a}_{in}^\dagger \hat{a}_{in} \rangle$ as the total flux of photons in the input field $|\alpha\rangle$. Using this in Eq 8, the weak excitation constraint thus puts a limit on $|\alpha|^2$ given by

$$\frac{|\alpha|^2}{\tau_p} \ll \frac{g^2}{\kappa} + \frac{\kappa \delta_1^2}{g^2} \quad (9)$$

where τ_p is the pulse width of the laser.

From Eq 9, we see that when there is no detuning δ_1 , the flux of photons in the input field $|\alpha\rangle$ should be less than the modified lifetime of the QD within the cavity $\frac{g^2}{\kappa}$. This is understandable because, if the first photon excites the QD and the second photon comes in before the QD has decayed, we will no longer be in the weak excitation limit. However, if the QD is off resonant from the cavity with detuning δ_1 , not all the light that comes in couples to the QD. Therefore, we will be able to pump the QDs with much more power before we exceed the weak excitation limit. This is given by the detuning dependent term $\frac{\kappa \delta_1^2}{g^2}$ in Eq 9.

Eq 9 conveys more than the weak excitation limit of $|\alpha\rangle$. If we apply the matching condition $\alpha r_1^g = \beta r_2^g$ in Eq 9, we obtain a limit on the flux of photons in the input field $|\beta\rangle$ given by

$$\frac{|\beta|^2}{\tau_p} \ll \frac{g^2}{\kappa} + \frac{\kappa\delta_2^2}{g^2} \quad (10)$$

We recognize this as the weak excitation limit equation for the field $|\beta\rangle$ which we would have obtained had we used the Heisenberg's equations of motion for cavity-dipole system 2. This implies that if we pick $|\alpha\rangle$ such that it satisfies the weak excitation limit of cavity-dipole system 1, the matching condition automatically ensures that the flux of photons in $|\beta\rangle$ is within the weak excitation limit of cavity-dipole 2.

Note that by making τ_p sufficiently long, we can always ensure that the system is in the weak excitation limit and that nonlinearities do not contribute. However, because we are using longer pulses the entanglement rate is reduced. The rate of entanglement generation is proportional to the rate at which the cavity reflects photons, given by $R = |\alpha r_1^g|^2/\tau_p$. Using the upper limit on $|\alpha|^2/\tau_p$ from Eq 9 and cavity reflectivity r_1^g from Eq 2, we get

$$R \ll \frac{g^2}{\kappa} \quad (11)$$

The above equation implies that the system will remain in the linear weak excitation limit provided that the rate of reflected photons is less than 1 photon per modified lifetime of the dipole. Note that this result is true regardless of the detunings, and is therefore valid in all cases.

It is instructive to compare the limits on the entanglement rate imposed by nonlinearities to the limits imposed by which-path information given in Section 3. The analysis of higher order photon numbers in the previous section showed that reflected photons $|\alpha r_1^g| \ll 1$ to have a high fidelity entangled state between the QDs. In contrast, the analysis of weak excitation limit in this section puts an upper bound on the rate of the input photons in $|\alpha\rangle$ and $|\beta\rangle$ given by $|\alpha r_1^g|^2/\tau_p \ll g^2/\kappa$. Thus, the two analyses are fundamentally different in that one limits the total number of input photons and the other limits the rate of incoming photons. Although one might expect the nonlinear limit analyzed in section 4 to be important, it turns out that the analysis of section 3 is more restrictive, and is therefore the important limit to consider. To understand why, we first note that nonlinearities can

always be suppressed by increasing the pulse duration τ_p . No matter how many photons we inject into the system, if we make the pulses sufficiently long we will always be in the weak excitation limit. In contrast, which-path information does not depend on pulse duration, and therefore cannot be suppressed. Furthermore, in order to stay in the monochromatic limit (i.e. to use the single frequency approximation) it has been shown in previous work that the pulse duration must be longer than the modified spontaneous emission lifetime of the dipole[17]. If we combine this with the results of section 3, which state that the number of reflected photons $|\alpha r_1^g|^2 \ll 1$, these two conditions already constrain us to work in the regime where the $|\alpha r_1^g|^2 / \tau_p \ll g^2 / \kappa$. Thus, we expect the entanglement to decohere due to which-path information before the nonlinear behavior in section 4 is observed. For this reason deviation from weak excitation does not pose any additional restrictions to the protocol that were not already present in the linear scattering regime.

V. 5. EFFECTS OF CAVITY DETUNING

In previous sections, we considered the idealized case where both the cavities had identical resonant frequencies. However in realistic systems, this will not be the case. Fabrication imperfections may lead to slightly different resonances for the two cavities. Clearly, if even a small amount of mismatch between the cavities were to result in no entanglement, the usefulness of our protocol would be questionable. Thus, it is important to consider how sensitive the protocol is to cavity resonance mismatch.

Now let's consider the case where the two cavities do not have the same resonant frequency. The analysis of the protocol in the presence of cavity detuning becomes involved for two reasons. First, it is no longer clear which frequency we should use for the coherent fields $|\alpha\rangle$ and $|\beta\rangle$. We do not know whether to place it on resonance with one of the cavities or somewhere in between. This can depend on both the cavity separation $\Delta\omega_s$ and dipole detunings δ_1 and δ_2 .

Second, the matching condition used in the previous section $\alpha r_1^g = \beta r_2^g$, is not guaranteed to be optimal. If a detection event is observed in detector $\hat{\mathbf{d}}_2$, then the state of the two QDs is

$$\begin{aligned} |\Psi_f\rangle_{dipoles} = & \frac{1}{N} [(\alpha r_1^g - \beta r_2^g)|gg\rangle + (\alpha r_1^m - \beta r_2^m)|mm\rangle \\ & + \alpha r_1^m|mg\rangle - \beta r_2^m|gm\rangle] \end{aligned} \quad (12)$$

where $N^2 = |\alpha r_1^m - \beta r_2^m|^2 + |\alpha r_1^m|^2 + |\beta r_2^m|^2$. The matching condition $\alpha r_1^g = \beta r_2^g$ ensures that we do not have any detection at $\hat{\mathbf{d}}_2$ if both the dipoles are in the state $|g\rangle$. However, the field amplitude at $\hat{\mathbf{d}}_2$ if both the dipoles are in the state $|m\rangle$ i.e. $(\alpha r_1^m - \beta r_2^m)$ is not compensated. This results in imperfect destructive interference at detector $\hat{\mathbf{d}}_2$. Thus, there is a small probability of detection at $\hat{\mathbf{d}}_2$ when both the dipoles are in state $|m\rangle$. This causes a loss of fidelity. In order to obtain the state that comes closest to the desired final entangled state, we must optimize the fidelity with respect to ω , α and β .

For calculating the effects of cavity detuning, we choose the frequency midway between the two cavity frequencies as the reference frequency Δ_{ref} . Based on this reference frequency, $\omega_1 = -\Delta\omega_s/2$ and $\omega_2 = \Delta\omega_s/2$. Also, it will be easier if we define the dipole detunings in terms of the reference frequency rather than the cavity frequencies. We define $\Delta_1 = \delta_1 + \omega_1$ and $\Delta_2 = \delta_2 + \omega_2$, which are the dipole detunings of dipoles 1 and 2 with respect to the reference frequency located midway between the two cavities. These definitions ensure that when increasing the cavity separation $\Delta\omega_s$ we do not affect the QDs. This is important because we can obtain information about the effects of cavity detuning alone by making these definitions.

Figure 4 plots the dependence of fidelity on the laser frequency for several different values of Δ_1 . The cavity separation $\Delta\omega_s = \omega_2 - \omega_1$ is set to 50 GHz, and $\Delta_2 = 0.25\kappa$. The figure is optimized over the real and imaginary parts of $\frac{\alpha}{\beta}$. The value of the maximum fidelity for the three curves occurs at three different frequencies. The frequency at which we get maximum fidelity is the optimal frequency ω . The fidelity at that frequency is the maximum fidelity that can be obtained for that particular configuration of $\Delta\omega_s$, Δ_1 and Δ_2 .

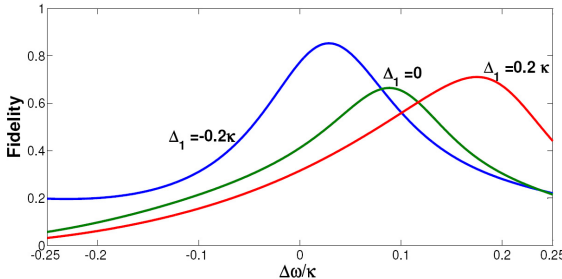


FIG. 4: a) Fidelity as a function of laser frequency for different values of Δ_1 . Optimization is performed over the real and imaginary parts of $\frac{\alpha}{\beta}$. Cavity separation $\Delta\omega_s$ is set to 50 GHz and $\Delta_2 = 0.25\kappa$ GHz

In Fig. 5, we plot optimized fidelity as a function of cavity detuning $\Delta\omega_s$ for different values of Δ_1 with $\Delta_2 = 0$. When $\Delta\omega_s = 0$, which represents the case when there is no cavity detuning, fidelity is 1. As the two cavities move apart, the spectra of the two cavities no longer overlap. Thus, there is a small probability of photon detection at $\hat{\mathbf{d}}_2$ when the dipoles are in the state $|mm\rangle$. This results in a loss of fidelity. Surprisingly, however, the fidelity does not continue to decrease, but instead increases back to 1 at some value of $\Delta\omega_s$.

As we keep increasing $\Delta\omega_s$ further, for a certain value of the laser frequency ω , both r_1^g and r_2^g are 0. If a detection event is observed in detector $\hat{\mathbf{d}}_2$, then the state of the two QDs collapses to

$$|\Psi_f\rangle_{dipoles} = \frac{1}{N}[(\alpha r_1^m - \beta r_2^m)|mm\rangle + \alpha r_1^m|mg\rangle - \beta r_2^m|gm\rangle] \quad (13)$$

where $N^2 = |\alpha r_1^m - \beta r_2^m|^2 + |\alpha r_1^m|^2 + |\beta r_2^m|^2$. In this special case there is a second matching condition, given by $\alpha r_1^m = \beta r_2^m$, that again projects the two dipoles onto $|\Psi_-\rangle = (|gm\rangle - |mg\rangle)/\sqrt{2}$. It is this second matching condition that results in the fidelity of 1 at the second peak. Our optimization algorithm naturally detects these two optimal regions, and gives us the best performance in the intermediate regime. Thus, given any set of operating conditions we have the ability to determine the best set of amplitudes and input frequencies. We note that in many cases fidelities exceeding 0.95 can be achieved even with an 60 GHz detuning, which is more than half a cavity linewidth. The fabrication of cavities with resonance frequencies that are repeatable within a linewidth is well within current technological capabilities.

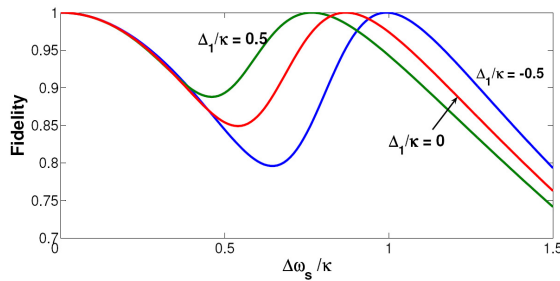


FIG. 5: a) Optimized fidelity as a function of $\Delta\omega_s$ for different values of Δ_1 . $\Delta_2 = 0$

We can also consider what happens when we have both cavity detuning and dipole detuning. In Fig. 6, we plot optimized fidelity as a function of cavity detuning $\Delta\omega_s$, and dipole detuning Δ_1 . A maximum fidelity of 1 is obtained when $\Delta\omega_s = 0$, which represents the case

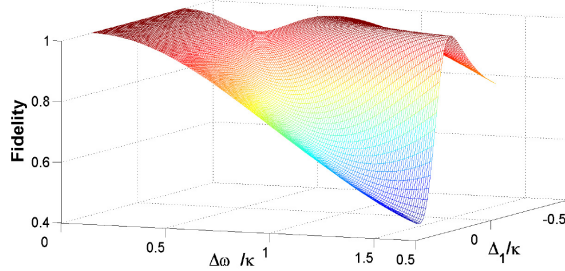


FIG. 6: (a) Fidelity as a function of cavity separations $\Delta\omega_s$ and dipole detuning Δ_1

when the two cavities have the same resonant frequency. For $\Delta\omega_s < g$ (where $g=20\text{GHz}$ in the plot) the fidelity is largely independent of the detuning Δ_1 and is only determined by cavity separation. When $\Delta\omega_s$ becomes larger, fidelity increases again due to the second matching condition and a dependence on the dipole detuning now becomes apparent. This dependence on detuning comes about from the fact that the second matching condition is a function of Δ_1 , as illustrated in Fig. 5. From Fig 6, fidelity is over 0.75 for a cavity linewidth separation(100 GHz) of the cavities even over a wide range of dipole detunings. Thus, we can use the protocol to obtain high fidelities even if the cavities and dipoles are detuned.

VI. 6. EXCITON-BIEXCITON IMPLEMENTATION

The protocol to generate entanglement between two QDs relies on considering the QD as a three level system. One of the ways to implement this three level system is by making use of the excitonic and biexcitonic transitions. A QD consists of three states: the ground state, an exciton state X consisting of a single electron-hole pair within the QD and a biexciton state XX which is formed when two electron-hole pairs are trapped inside the QD. The recombination of an electron-hole pair in the XX state generates the biexciton XX photon. Similarly, the recombination of an electron-hole pair in X state generates the X photon. The X and XX photons have different energies due to the coulomb and exchange interactions between the carriers. The typical energy separation between the two lines is 1mev[36]. Thus, we can make use of this difference in energies to spectrally isolate the two lines.

The schematic of the QD as a three level system is shown in Fig 7. We identify the three states of the QD as the ground, X and XX states. We are free to assign these three states as $|g\rangle$, $|m\rangle$ and $|e\rangle$ in a variety of different combinations. In fact, there are several ways

to assign these levels, but probably the most convenient approach is given in the inset of Fig 7. In the figure we have identified the ground state of the QD as state $|m\rangle$, the single exciton state as state $|g\rangle$, and the bi-exciton state as state $|e\rangle$. This choice of the level configuration has a number of advantages. First, single qubit operations between $|g\rangle$ and $|m\rangle$ can be directly applied by pulses resonant with the single exciton transition. Second, by placing the bi-exciton transition on resonance with the cavity, we can enhance the exciton to bi-exciton transition to get DIT, while at the same time suppressing the single exciton lifetime in order to increase the coherence time of the qubit. This is illustrated in Fig 7.

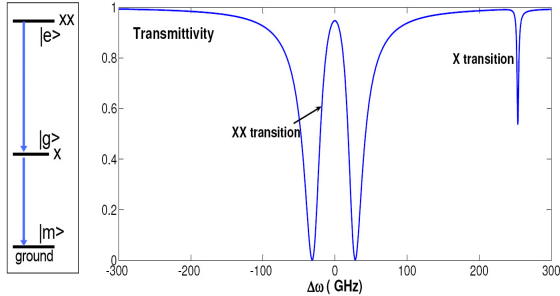


FIG. 7: QD as a three level system

We assume the biexciton transition to be on resonance with the cavity frequency. This is indicated in Fig 7 where the XX transition is in the middle of the cavity spectrum. The X transition line is detuned from the cavity by δ_X . The vacuum Rabi frequencies of X and XX transitions are given by g_X and g_{XX} respectively. Similarly, the decay rates of the two transitions is given by γ_X and γ_{XX} respectively.

In the exciton bi-exciton scheme the degree of cavity enhancement directly impacts our ability to create an entangled state. This is because both the exciton and bi-exciton are strongly radiative states, and the only way to enhance one while suppressing the other is to use cavity lifetime modification. In other qubit implementations, such as dark state excitons[26], this is not as much of a problem because selection rules make the dark exciton long lived regardless of cavity. To quantitatively address this issue, we first calculate the coherence time of the exciton state which is given by solving for the decay rate of σ_- in Eq. 1. The coherence time of the qubit is given by

$$\Gamma_X = \frac{g_X^2 \kappa}{\delta_X^2 + \kappa^2} + \gamma_X + \frac{1}{T_2} \quad (14)$$

where we have added the dipole dephasing rate $1/T_2$ to the decay rate. From the above

equation one can see that increasing δ_X decreases the decoherence rate until it finally saturates at a minimum value of $\gamma_X + 1/T_2$. At this point, increasing the detuning of the exciton will not help as we are limited by non-radiative and dephasing processes.

The coherence time of the dipole should be compared to an appropriate time scale in order to determine if entanglement can be generated. Although there are a number of different factors that should be considered in this comparison, the minimum requirement for generating entanglement is that the duration of the entangling pulse should be shorter than the coherence time of the qubit. If this is not the case, the qubit will begin to decohere before the entangling pulse has finished interacting with the cavity-dipole system, and there is no hope of generating high-fidelity entanglement. In previous work in Ref [17], it has been shown that when the pulse is resonant with the dipole, it must be much longer than the modified spontaneous emission lifetime of the dipole in order to be monochromatic. Thus, in the worst case when the dipole is resonant with the cavity we need $1/\tau_p \ll g_{XX}^2/\kappa$. We thus argue that an important figure of merit is the ratio of the coherence time of the qubit to the entanglement pulse width, given by

$$N_{ent} = \frac{g_{XX}^2}{\kappa\Gamma_X} \quad (15)$$

This ratio determines the maximum number of entanglements that can be performed before the system decoheres. If $N_{ent} > 1$, there is enough time for the pulses to finish their interaction with the QDs before the system has decohered. Otherwise, the QDs will start to decohere before the pulses have finished their interaction and high fidelity entanglement will be impossible.

For calculations, we choose experimental values taken from the paper of Hennessy et. al. [37] which investigates the coupling of an Indium Arsenide (InAs) quantum dot coupled to a photonic crystal cavity patterned in Gallium Arsenide (GaAs) by electron beam lithography. This experimental work reports $g=20$ GHz and cavity linewidth of 25 GHz which corresponds to a Q of 13300. However, the cavity linewidth is the bare cavity Q which corresponds to the decay into the leaky modes. In order to achieve critical coupling with the cavity, we need another in-plane mode with a decay rate equal to the bare cavity decay rate. This mode can be implemented in a photonic crystal as a waveguide coupled to the cavity. Thus, the total decay rate of the cavity is double that of the bare cavity decay rate. Hence, we use $\kappa = 50$ GHz in our calculations. We use $g_X = g_{XX} = g$. For values of T_2 we use 2 ns, which are

appropriate values for InAs QDs[38]. For these values, g_{XX}^2/κ is 8 GHz, Γ_x is 0.93 GHz and N_{ent} is 8.6. The fact that $N_{ent} > 1$ ensures that we can complete an entanglement operation well before the QDs have decohered.

For a cavity linewidth of 50 GHz, the exciton line lies outside the cavity spectrum($\delta_X = 250$ GHz). However, the exciton line still couples to the cavity and we cannot ignore the presence of the extra transition coupled to the cavity. So, we cannot substitute for g as 0 in Eq 2 in order to obtain the cavity reflection and transmission equations when the QD is in state $|m\rangle$. We need to use the vacuum Rabi frequency as the value for g to obtain the values of r_1^m , t_1^m , r_2^m and t_2^m . The changes in the transmission and reflection coefficients will modify the final state of the QDs and hence the fidelity of the system.

In general we cannot assume that the XX transition is not detuned from the cavity spectrum. In order to see how robust the biexciton-exciton protocol is dipole detunings, we define the detunings of the XX transition lines from their cavities as δ_{XX1} and δ_{XX2} . In Fig 8 we plot the dependence of fidelity on dipole detunings δ_{XX1} and δ_{XX2} for the above case. For both $\delta_{XX1} = 0$ and $\delta_{XX2} = 0$, fidelity is 1 as expected. When we increase δ_{XX1} and δ_{XX2} , the transmission and reflection coefficients are modified due to the coupling of the X transition to the cavity. This lowers the fidelity of the output state. The drop in fidelity is gradual and for a cavity linewidth separation of the dipoles from the cavity resonance(50 GHz), fidelity drops to only 0.96. As we further increase the detunings to 100 GHz, fidelity drops to 0.85. Thus, even for large detunings between the cavities and the dipoles, reasonable high fidelity(0.85) states of the QDs can be obtained. Thus, the exciton-biexciton scheme can be used to create entanglement between QDs even if the exciton line couples to the cavity. The performance of the protocol can be further improved by fabricating cavities with high quality factors.

VII. 7. CONCLUSIONS

In conclusion, we have shown that one can achieve high fidelity entangled states between two dipoles, even when their emission frequencies are different. The method is robust to dipole and cavity frequency mismatch. Efficiency loss for a cavity linewidth change in dipole detuning is about 50% for a constant fidelity. Therefore, relatively high fidelity can be obtained over a large range of dipole detunings without significant loss of efficiency. The

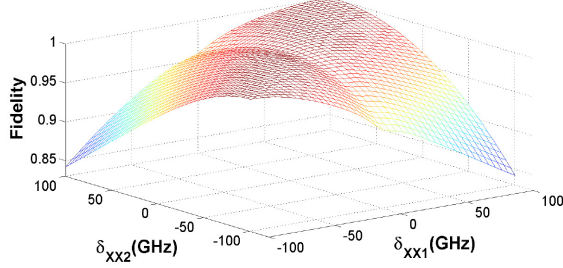


FIG. 8: Fidelity as a function of dipole detunings δ_1 and δ_2 for the exciton-biexciton model of a QD

development of protocols that are robust to these imperfections is extremely important for semiconductor based implementations of quantum networks.

The authors acknowledge the support of Army Research Office under the Grant No. W911NF0710427.

VIII. APPENDIX

The input coherent fields are $|\alpha\rangle$ and $|\beta\rangle$. Both the dipoles are initialized in a superposition of states $|g\rangle$ and $|m\rangle$. Thus, the initial state of the system is

$$|\Psi_i\rangle = |\alpha\rangle|\beta\rangle(|g\rangle + |m\rangle)(|g\rangle + |m\rangle)/2 \quad (16)$$

The coherent states can be replaced by their corresponding displacement operators to account for all order of photon numbers. Thus,

$$|\Psi_i\rangle = \frac{1}{2} e^{(\alpha \hat{a}_{in}^\dagger - \alpha^* \hat{a}_{in})} |0\rangle_{a_{in}} e^{(\beta \hat{c}_{in}^\dagger - \beta^* \hat{c}_{in})} |0\rangle_{c_{in}} (|gg\rangle + |gm\rangle + |mg\rangle + |mm\rangle) \quad (17)$$

The input fields after interactions with the cavity-dipole systems are transformed according to Eq 2. Thus, when the dipoles are in state $|gg\rangle$

$$\begin{aligned} \hat{a}_{in}^\dagger &\rightarrow r_1^g \hat{a}_{out}^\dagger + t_1^g \hat{b}_{out}^\dagger \\ \hat{c}_{in}^\dagger &\rightarrow r_2^g \hat{c}_{out}^\dagger + t_2^g \hat{d}_{out}^\dagger \end{aligned} \quad (18)$$

Similar transformation equations apply when the dipoles are in the states $|gm\rangle$, $|mg\rangle$ and $|mm\rangle$. The reflected field from the two cavities is mixed on a 50/50 beamsplitter that applies the transformation:

$$\begin{aligned}\hat{a}_{out}^\dagger &\rightarrow (\hat{d}_1 + \hat{d}_2)/\sqrt{2} \\ \hat{c}_{out}^\dagger &\rightarrow (\hat{d}_1 - \hat{d}_2)/\sqrt{2}\end{aligned}\tag{19}$$

Applying the cavity and beamsplitter transformations on the initial state $|\Psi_i\rangle$ we get

$$\begin{aligned}|\Psi_{gg}\rangle &= D\left(\frac{\alpha r_1^g + \beta r_2^g}{\sqrt{2}}\right) D\left(\frac{\alpha r_1^g - \beta r_2^g}{\sqrt{2}}\right) D(\alpha t_1^g) D(\beta t_2^g) \\ &\quad |0\rangle_{d_1, d_2, b_{out}, d_{out}} |gg\rangle\end{aligned}\tag{20}$$

$|\Psi_{gg}\rangle$ is the state of the output modes for the dipoles in state $|gg\rangle$. This state can be split up into the modes of detector \hat{d}_1 , \hat{b}_{out} and \hat{d}_{out} and detector \hat{d}_2 . Thus,

$$\begin{aligned}|\Psi_{gg}\rangle &= |\psi_{gg}\rangle |\mu_{gg}\rangle |gg\rangle \\ |\psi_{gg}\rangle &= D\left(\frac{\alpha r_1^g + \beta r_2^g}{\sqrt{2}}\right) D(\alpha t_1^g) D(\beta t_2^g) |0\rangle_{d_1, b_{out}, d_{out}} \\ |\mu_{gg}\rangle &= D\left(\frac{\alpha r_1^g - \beta r_2^g}{\sqrt{2}}\right) |0\rangle_{d_2}\end{aligned}\tag{21}$$

$|\psi_{gg}\rangle$ is the state of the output modes at detector \hat{d}_1 and the transmitted modes \hat{b}_{out} and \hat{d}_{out} when the dipoles are in state $|gg\rangle$. $|\mu_{gg}\rangle$ is the field amplitude at detector \hat{d}_2 when the dipoles are in state $|gg\rangle$. Similarly, we can obtain the field amplitudes $|\Psi_{gm}\rangle$, $|\Psi_{mg}\rangle$ and $|\Psi_{mm}\rangle$ when the dipoles are in states $|gm\rangle$, $|mg\rangle$ and $|mm\rangle$. The final state of the system is given by

$$|\Psi_f\rangle = |\Psi_{gg}\rangle + |\Psi_{gm}\rangle + |\Psi_{mg}\rangle + |\Psi_{mm}\rangle\tag{22}$$

These states $|\Psi_{gm}\rangle$, $|\Psi_{mg}\rangle$ and $|\Psi_{mm}\rangle$ can be further decomposed on similar lines to Eq 21 to obtain the field amplitudes $|\psi_{gm}\rangle$ and $|\mu_{gm}\rangle$, $|\psi_{mg}\rangle$ and $|\mu_{mg}\rangle$ and $|\psi_{mm}\rangle$ and $|\mu_{mm}\rangle$ respectively.

We define the projection matrix M as $\sum_{n=1}^{\infty} |n\rangle_{d_2} \langle n|$. M can also be written as

$$\begin{aligned}
M &= \sum_{n=0}^{\infty} |n\rangle_{d_2} \langle n| - |0\rangle_{d_2} \langle 0| \\
&= I - |0\rangle_{d_2} \langle 0|
\end{aligned} \tag{23}$$

$$\rho_{dipoles} = \frac{tr_{(\text{fields})}\{\langle M|\Psi_f\rangle\langle\Psi_f|M\rangle\}}{tr_{(\text{dipoles\&fields})}\{\langle M|\Psi_f\rangle\langle\Psi_f|M\rangle\}} \tag{24}$$

$$\begin{aligned}
F &= \langle\Psi_-|\rho_{dipoles}|\Psi_-\rangle \\
&= \langle\Psi_-|\frac{tr_{(\text{fields})}\{\langle M|\Psi_f\rangle\langle\Psi_f|M\rangle\}}{tr_{(\text{dipoles\&fields})}\{\langle M|\Psi_f\rangle\langle\Psi_f|M\rangle\}}|\Psi_-\rangle
\end{aligned} \tag{25}$$

The denominator is the probability of getting a detection at detector $\hat{\mathbf{d}}_2$. We identify this as efficiency η .

$$\begin{aligned}
F &= \langle\Psi_-|\rho_{dipoles}|\Psi_-\rangle \\
&= \langle\Psi_-|\frac{tr_{(\text{fields})}\{|\Psi_f\rangle\langle\Psi_f|\} - tr_{(\text{fields})}\{\langle 0|\Psi_f\rangle\langle\Psi_f|0\rangle_{d_2}\}}{\eta}|\Psi_-\rangle \\
&= \frac{F_1 - F_2}{\eta}
\end{aligned} \tag{26}$$

The individual terms can be evaluated to give

$$\begin{aligned}
F_1 &= \frac{1}{4} - \frac{\langle\Psi_{gm}|\Psi_{mg}\rangle}{2} - \frac{\langle\Psi_{mg}|\Psi_{gm}\rangle}{2} \\
F_2 &= \frac{1}{8}e^{-|\mu_{gm}|^2} + \frac{1}{8}e^{-|\mu_{mg}|^2} - \frac{1}{2}e^{-(|\mu_{gm}|^2+|\mu_{mg}|^2)/2}\langle\psi_{mg}|\psi_{gm}\rangle \\
&\quad - \frac{1}{2}e^{-(|\mu_{gm}|^2+|\mu_{mg}|^2)/2}\langle\psi_{gm}|\psi_{mg}\rangle \\
\eta &= \frac{1}{4}[e^{-\mu_{gg}^2} + e^{-\mu_{gm}^2} + e^{-\mu_{mg}^2} + e^{-\mu_{mm}^2}]
\end{aligned} \tag{27}$$

Thus, the complete expression for fidelity and efficiency can be obtained.

[1] A. K. Ekert, Phys. Rev. Lett. **67**, 661 (1991).

[2] T. Jennewein, C. Simon, G. Weihs, H. Weinfurter, and A. Zeilinger, Phys. Rev. Lett. **84**, 4729 (2000).

- [3] C. H. Bennett ,G. Brassard, C. Cr  peau, R. Jozsa, A. Peresand W.K. Wooters, Phys. Rev. Lett. **70**, 1895 (1993).
- [4] D. Bouwmeester et al., Nature **390**, 595 (1997).
- [5] W. T. Buttler,R.J. Hughes, P.G. Kwiat,S.K. Lamoreaux, G.G. Luther et al., Phys. Rev. Lett. **81**, 3283 (1998).
- [6] K. Mattle, H. Weinfurter, P. G. Kwiat and A. Zeilinger, Phys. Rev. Lett. **76**, 4656 (1996).
- [7] H.-J. Briegel, W. D  r, J. I. Cirac and P. Zoller, Phys. Rev. Lett. **81**, 5932 (1998).
- [8] W. D  r, H.-J. Briegel, J. I. Cirac and P. Zoller, Phys. Rev. A **59**, 169 (1999).
- [9] P. G. Kwiat,K. Mattle, H. WeinfurterandA. Zeilinger, , Phys. Rev. Lett. **75**, 4337 (1995).
- [10] D. Jaksch, H.-J. Briegel, J. I. Cirac, C. W. Gardiner and P. Zoller, Phys. Rev. Lett. **82**, 1975 (1999).
- [11] L.-M. Duan, M. D. Lukin, J. I. Cirac and P. Zoller, Nature **414**, 413 (2001).
- [12] L. Childress, J.M. Taylor, A.S. Sorenson and M.D. Lukin, Phys. Rev. Lett. **96**070504 (2006).
- [13] S.D. Barrett and P. Kok, Phys. Rev. A **71**, 060310(R) (2005).
- [14] P. van Loock et al., Phys. Rev. Lett. **96**, 240501 (2006).
- [15] D. Englund , A. Farson , B. Zhang , Y. Yamamoto and J. Vuckovi , Optics Express **15**, 5550 (2007).
- [16] D. Englund et al., Phys. Rev. Lett. **95**, 013904 (2005).
- [17] E. Waks and J. Vuckovi , Phys. Rev. Lett. **96**, 153601 (2006).
- [18] J. M. G  rard, B. Sermage, B. Gayral, B. Legrand ,E. Costard and V. Thiery-Mieg, Phys. Rev. Lett. **81**, 1110 (1998).
- [19] E. Moreau, I. Robert, J. M. G  rard, I. Abram, L. Manin and V. Thiery-Mieg, App. Phys. Lett. **79**, 2865 (2001).
- [20] T. Yoshie et al., Nature **432**, 200-203 (2004).
- [21] A. Badolato et al., Science **308**, 1158 (2005).
- [22] J.P. Reithmaier et al., Nature **432**, 197 (2004).
- [23] D. Englund et al., Nature **450**, 857 (2007).
- [24] K. Srinivasan and O. Painter , Nature **450**, 862 (2007).
- [25] C. Santori et al., Phys. Rev. Lett. **86**, 1502-1505 (2001).
- [26] R.M. Stevenson et al., Phys. Rev. B. **73**, 033306 (2006).
- [27] E.A. Stinaff, Science **311**, 636 (2006).

- [28] Dan Gammon, *Nature Physics* **3**, 761 (2007).
- [29] K.-M.C Fu, *Phys. Rev. Lett.* **95**, 187405 (2005).
- [30] C. Santori et al., *Phys. Rev. Lett.* **97**, 247401 (2006).
- [31] K. Pieter and L.W. Brendon, *Nature* **444**, 49 (2006).
- [32] T.H. Stievater et al., *Phys. Rev. Lett.* **87**, 133603 (2001).
- [33] D. Walls and G. Milburn, *Quantum Optics* (Springer, Berlin, 1994).
- [34] D. Englund et al., arXiv:quant-ph/0501091. (2005).
- [35] A. Aufféves-Garnier et al., *Phys. Rev. A* **75**, 053823 (2007).
- [36] P. Alonso-González et al., *App. Phy. Lett.* **91**, 163104 (2007).
- [37] K. Hennessy et al., *Nature* **445**, 896 (2007).
- [38] W. Langbein et al., *Phys. Rev. B* **70**, 033301 (2004).